FLOOD RISK MONITORING AROUND PART OF THE NIGER DELTA BASIN OF NIGERIA

Ahmadu, A. A.[1], Dodo, J. D.[2] & Ojigi, M. L.[2]

[1]Department of Geomatics, Faculty of Environmental Design, Ahmadu Bello University (ABU), Zaria. Kaduna State, Nigeria.
[2]Center for Geodesy and Geodynamics, Toro Bauchi State, Nigeria.
Correspondence to: (aliahmaduabubakarmsc@gmail.com) & (jddodo@gmail.com)

ABSTRACT

Different environmental geo-hazard events on the society are seriously manifesting by the extent of flood which that influenced by climate change variables. This research is tailored on investigating the dynamics of frequently occurring natural flood disaster. Recently launch Sentinel-1 SAR satellite constellation was adopted for temporal feature extraction and extent assessments over the study area. Methodology adopted involves Binarization (Thresholding) techniques, suitable pixel intensity through Band Maths to calculate and extract water accumulation with-in the Area of Interest (AOI). Result obtained shows that, number of scenes has no influenced on the expected outcome with a gradual increase in flood geo-hazard from September, 2017 (10.49345%) to May, 2018 (12.6057%) and a slight drop in May, 2019 (11.47714%). Flood events possess a gradual progressive increase over time with that of October, 2022 as high as (12.29319%). It was observed that May, 2018 have the highest percentage of water catchments area (12.6057%) with the highest percentage of flood geo-hazard, then October, 2020 (12.29319%), then May, 2019 (11.47714%) and September, 2017 (10.49345%). Rate of water accumulation over the AOI was predicted with an extension to October, 2022. It was evident that flood event is a gradually accumulated and continuous geo-hazard event. Being a continuous phenomenon, over a period of time, it however flooded the solid part of the earth surface where most human activity such as places reserves for farming and dwelling. It could be seen that flood rate is not constant because other activities could also contribute immensely towards increasing flood geo-hazard. The recommended that study of geo-hazard events should be investigated at an interval adopting a space base approach with numerous advantages.

Key words: Binarization, Band Maths, SLC to GRDH, Water Mask, Water Accuracy, Flood Geo-hazard and Rate of Water Accumulation

1.0 Introduction

Influence of climate change has been a major thread on associated environment and the society at large leading to all categories of geo-hazard events in so many ways, approaches and perspectives. Among others, the intensity of hydrological cycle is leading to more and more extreme drought and precipitation events within and around the environment, society and eventually an increase in the frequency and extent of flood events as a result of water overflowing it bangs (World, 2016; Cazenave & Gonéri, 2013; Benjamin *et al*., 2018; Bioresita & Puissant, 2021). As it is the most frequently occurring natural geo-hazard events, insights into their occurrence and dynamics will be of innermost importance for an effective disaster management as well as for the calibration and validation of flood prediction models, and the optimization of spatial planning (Landuyt, Coillie, Vogels, Dewelde, & Verhoest, 2021; Bovenga, 2020; Li *et al*., 2022).

As was observed, optical sensors are hampered by cloud cover, which is often persistent during flood events, which make reliable measurement on the spatial occurrence of historical flood events obviously difficult (Younis, 2015; Artiola, Pepper, & Brusseau, 2004; Richards, Scheer, & William A. Holm, 2011; Rajakumari *et al*., 2021; Matgen *et al*., 2020; Sadek *et al*., 2020; Bioresita & Puissant, 2021; Cunha *et al*., 2011; Rajakumari *et al*., 2021; Bioresita & Puissant, 2021). Flooding is a global phenomenon, underlined by a range of source mechanisms, and widely considered as the most common natural hazard (Stefanidis and Stathis, 2013; Below and Wallemacq, 2018, Rajakumari *et al*., 2021, Matgen *et al*., 2020 and Sadek *et al*., 2020). Dartmouth Flood Observatory (DFO) made effort to collate and map inundation events as in Figure 1.0, showing flood occurrence totaling 3,129 since 2000. Given the global nature of flooding, sufficient in-situ monitoring is considered geographically impracticable and likely to be expensive, whilst nominally providing point measurements that have questionable use for understanding the dynamics of such an event (Maheu *et al*., 2003; Alsdorf *et al*., 2007; Rajakumari *et al*., 2021; Li *et al*., 2022). Hydrodynamic models were developed for most types of flooding with certain simulations which output flood extent, depth and velocity information (Teng *et al*., 2017; Rajakumari *et al*., 2021; Li *et al*., 2022). It was made clear that, there are natural and epistemic uncertainties with the development of hydrodynamic models which hamper and reduce confidence in their outputs (Merz and Thieken, 2005; Rajakumari *et al*., 2021; Li *et al*., 2022).

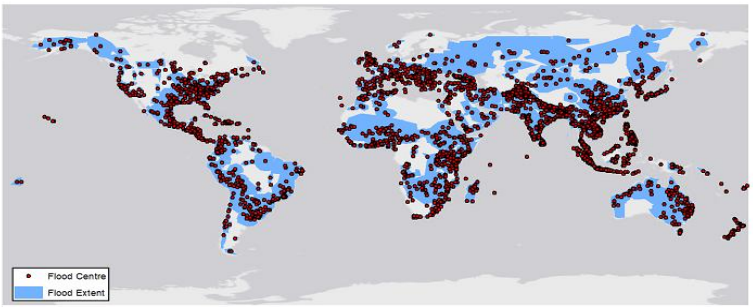

Figure 1.0 Centroid locations and impacted regions of floods event between 2000 and 2018 (n = 3129) recorded in DFO database

The records suggest there were over 390,000 fatalities from flooding during the period, with approximately 350 million people displaced (Clement, 2020). Urbanization and the replacement of natural land cover with impenetrable surfaces alter the storage and runoff properties by reducing infiltration and increasing surface runoff (Miller *et al*., 2014; Clement, 2020). Both mechanisms result in water moving faster into the river network, either overland flow or via man-made culverts and sewer systems, which subsequently increases the peak flows whilst reducing the lag time (Huang *et al*., 2008; Braud *et al*., 2013; Clement, 2020). Flood risk can be categorically made up of three components;

a. the probability and characteristics of the flood event,
b. the exposure of population and assets to the hazard, and
c. the extent on vulnerable community and its ability to cope with the impacts during and after the event (Jongman *et al*., 2012 and Clement, 2020).

1.1 ESA Copernicus Programme and the Sentinels Mission

European Commission (EC) and the European Space Agency (ESA) started the Copernicus programme in 2014, as a natural successor to the Global Monitoring for Environment and Security (GMES) programme (Clement, 2020). Earth observation satellites (EOS) provide efficient and suitable means to monitor wide variety of environmental variables (Huang *et al*., 2018; Clement, 2020), soil moisture (Gao *et al*., 2017), wetlands (Muro *et al*., 2016) and snow cover (Snapir *et al*., 2019). Recently launch satellites actually increases the quantity and quality of available data, improving the potential to monitor geo-hazard dynamic, environmental variables from space with the (ESA) Copernicus programme, including the Sentinel-1 SAR satellite constellation. Sentinel-1 satellite provides global imagery every 6-12 days at no cost to the end user (Clement, 2020; Matgen *et al*., 2020; Sadek *et al*., 2020). Additionally, satellite data has been used for post-event damage assessments and has helped inform flood risk mitigation and adaptation strategies (Bovolo and Bruzzone, 2007; Rahman and Di, 2017; Matgen *et al*., 2020; Martinis *et al*., 2017; Li *et al*., 2022).

2.0 Study Area

The study area is a part of Nigeria which form boundary to the south with the Atlantic Ocean (coastal water body), East with Cameron Republic, North with Niger Republic and West with Benin Republic. The study area is bounded between the following geographic location (5^0E to 8^0E) of the Meridian and (4^0N to 8.75^0N) of the Equator.

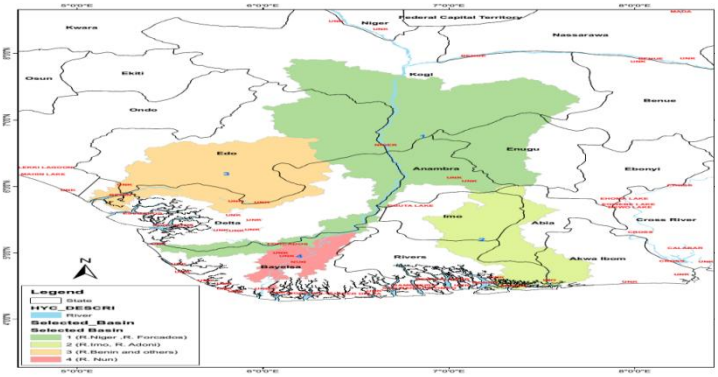

Figure 1.0 Map Part of Nigeria Showing the Study Area

3.0 Methodology

Approach to this study includes processing of SAR sentinel-1 image scenes for waterlog extraction, temporal feature extraction and extent assessments. Spatial information derived from the processed data was further integrated to assess the extent of water inundation over the study period and Area.

3.1 Materials and Method

Raw data used for this study are sentinel-1 single look complex (SLC), interferometric wide swath (IW) between 2016 and 2019 at an interval of three months (3) each year and GRDH, IW for 2022 (Earth data, 2019) as shown in table 2.0.

Table 2.0 Data set Characterastics (source: Mariana, 2010)

S/N	Dataset	Source	Purpose
1.	C-Band SLC wide-swath (IW) Sentinal-1A & B	Both descending and ascending satellite passes at https://nisar.jpl.nasa.gov of NASA-ISRO SAR Mission (NISAR)	Used to study the backscattering coefficient of the Surface Water and phase of the Radar sensor over the same scene

Satellite	Time of operation & Launch	Freq. Band	Polarization	Cycle and Days	Altitude (km)	Look angle, deg.	Swath width (km)	Resolution (m)
Sentinel-1Aand 1B	2014 and 2015	C	Dual	6-12	693	20-45	400	2

3.2 Data Acquisition

Data were acquired over the study area and period (2016 to 2019 and 2022) based on some features such as; size, processing, climate and weather variables. Data were acquired at an interval of three months for each year based on the seasonal behaviour (January, May and September). The acquisition considered the peak of river capture and the lowest level of river capture since most of the water source is rainfall from other part of the country and that of the study area.

3.3 Processing Approach

The research goal can be determined through the analysis and processing approach using desired data set. There are several approaches and software to be adopted for research of this nature. However, this research adopted the open-source free software known as Sentinel Application Tool Box (SNAP) through the following methodology approach as show in Figure.

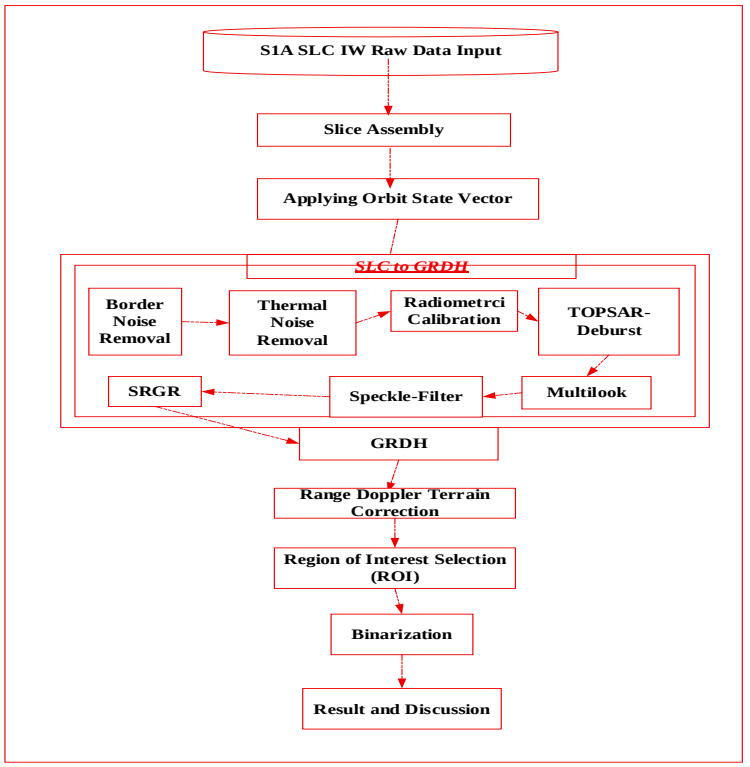

Figure 3.0: Flood event flow chart approach

3.4 Preprocessing

The first step of flood mapping analysis with SNAP is preprocessing. It starts with slice assembly of sentinel-1 Interferometric wide (IW) swath mode which is capable of operating up to 25 minutes. Expanding the IW swath into extra wide swath (EW) mode operating up to 60 minutes required the slice assembly of the image scene so as to have a concatenated horizontal exaggeration covering a wider ground area.

3.4.1 Orbit file application

The precise orbit state vector was applied to improve the geocoding of the product so as to have an accurate satellite positioning, timing and velocity. It was automatically applied in the processing software, sentinel application tool box (SNAP).

3.4.2 Sentinel-1 SLC to GRD

Data used for this study are Single Look Complex (SLC) which does not possess the amplitude band but possess the intensity and the complex band. The study is most sensitive to the

amplitude band; as such the SLC product is converted to a similar product, Ground Range Detection High Resolution (GRDH) product. The processes involved are;

a. Thermal Noise Removal
b. Calibration
c. Deburst and Merge of TOPS data
d. Multilooking
e. Speckle Filtering
f. Slant Range to Ground Range Conversion (SRGR)
g. Scaling to 16 bits
h. Updating metadata.

The bursts in all sub-swaths are seamlessly merged to form a single, contiguous, ground range, detected image. The inherent salt and pepper like texture (speckles) of SAR image which degrade it quality and make interpretation of features difficult were taking care of by adopting a suitable model developed by Lee during speckle filtering operation with a window size of 7 by 7 (Lee and Pottier, 2009).

3.4.3 Terrain Correction

Images not directly at the nadir location will experience certain magnitude of distortion. This approach compensates for these distortions so that the geometric representation of the image will be as close as possible to the real-world representation. Figure 3.1 outline the geometry of topographical distortions. Point **B** with an elevation **h** above the ellipsoid is image at position $B\not{\phi}$ in SAR image, though its real position is $B\not{\phi}$. The offset D_r between $B\not{\phi}$ and $B\not{\phi}$ exhibits the effect of topographic distortions.

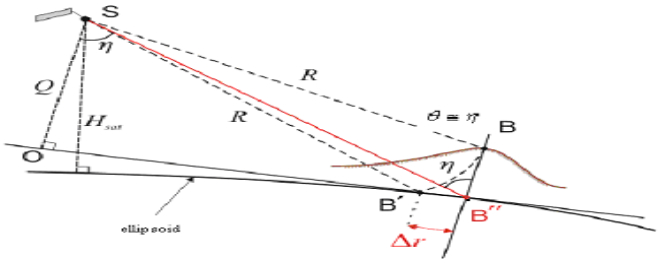

Figure 3.1 Doppler Terrain Effect

3.4.4 Area of Interest (AOI)

Since the image scene is wide covering far beyond the study area at large-scale making feature identification difficult, it calls for a concentration on the area of interest (AOI). Sub setting is adopted to clip the image to the region of interest as observed in Figure 1.0.

3.4.5 Binarization (Thresholding)

Creating water mask region is very crucial to actually delineate the extent of flood event. Water regions have a low back scattered coefficient than non-water regions because they create a smooth surface where the SAR signal is refracted according to Snell's law which makes it act as a spectral reflectance. Figure 3.2 with image A (Sigma band 0 scene) and B (Sigma band 0 scene in decibel (db)). The image B gives a sharp distinction between water body pixel and that of other features. The bell curve on the lower left side of the image scene B which have two spikes of the graph showing the intensity values for non-water pixels and the lower spike of the bell curve is for water pixel.

Figure 3.2 Pixel Intesity Values of Sigma0 A and B

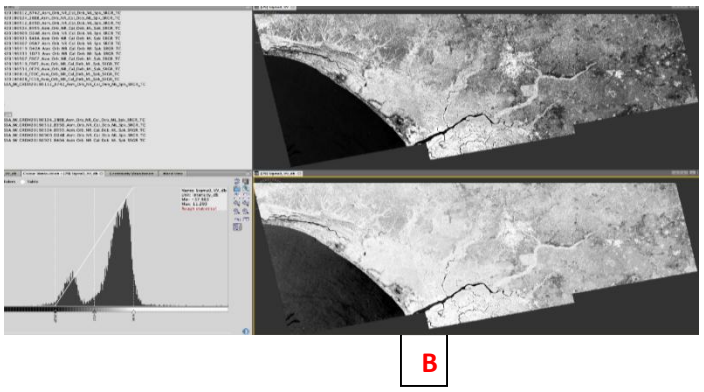

Based on this influence of scene A and B, the image is classified as water and non-water area by setting a threshold to create both classes through an approach known as binarization. Binarization is control and also depends on pixel values extracted from the image histogram and statistics. The image scene is converted to decibel units which enhance the pixel values thresholding and give a better separability in terms of pixel information with an improved speckle appearance. Polygon layer was used on the image scene to extract the water pixel intensity. Figure 3.3 shows the position of the polygon layer and the intensity values at the top left side of the Figure. The suitable intensity pixel value for water mask is extrapolated from the bell curve at the lower left side of the Figure.

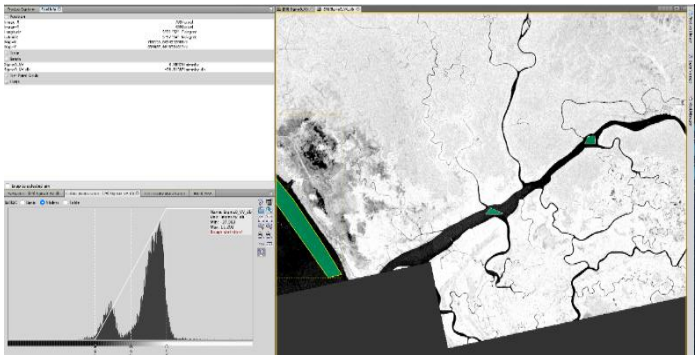

Figure 3.3 Polygon Layer Intensity Values used for Water Masking

The lower pixel values correspond to water body whereas the higher value from the bell curve histogram corresponds to other features within the scene. Having obtained suitable pixel intensity, the study used a Band Maths as another approach to

calculate and extract only water bodies with-in the image scene as shown in Figure 3.4;

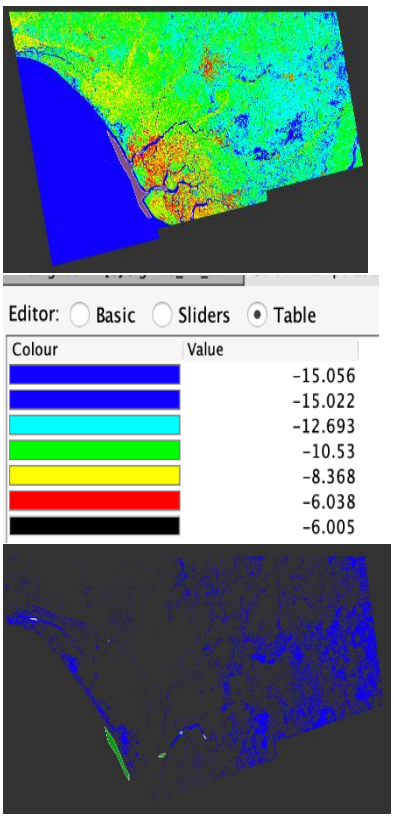

Figure 3.4 Water Mask of the Study Area

Figure 3.4 outlines the extent of water present with-in the study area. The image scene shows that the study area consists of river channels and water shades. It is indicated by the legend table of different colors indicating the extent of water shade. The region appearing in red are mostly built-up areas with the range of value -6.038 m predicting an expectation of flood event. The range of value shows the extent of water shade within the study area and foot print to flooding.

Figure 3.5 displayed and show the water mask accuracy with-in the study area. The Figure to the left shows the values corresponding to accuracy index in terms of total number of pixel present, mean value, sigma, coefficient of variation, threshold percentile and maximum error ellipse obtain from the processed result. The bell curve shows an indication for only water pixel intensity whereas the image in red shows the different thresholding values with P75, P80, P85 and P90 values outline in the Figure 3.5.

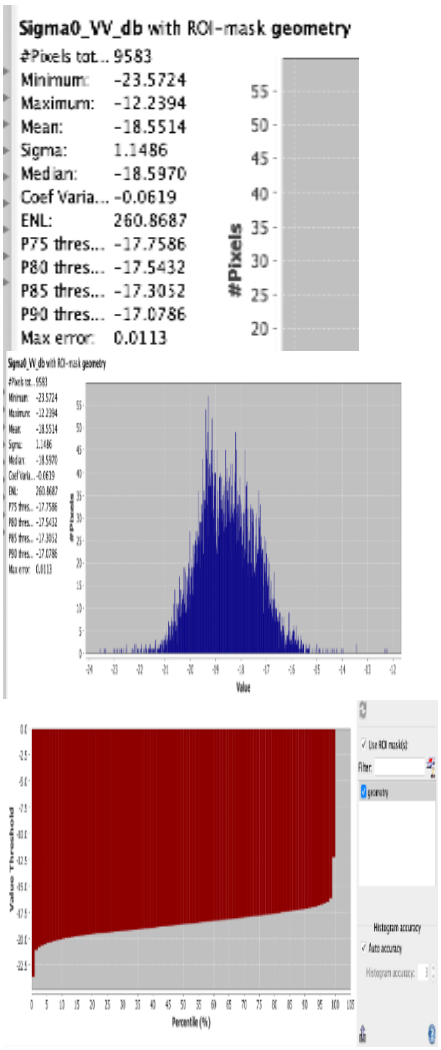

Figure 3.5 Statistical Information of the Water Mask

4.0 RESULTS AND DISCUSSION

4.1 Monthly Flood Water Monitoring

Figure 4.1 displayed the contrasting behavioral relationship between the parameters of flood monitoring over the study area and epoch. Figure 4.1A is a line plot showing a strong positive correlation between the number of active scenes, water accumulation (%) and the Sigma value of the process result. Figure 4.1B shows the intensity of accumulated water with regards to the number of scenes at monthly intervals for five years including only one month of October in 2022. It shows that, the least active scenes are in January 2016, then September 2019, with the least accumulated water coverage in percentage. The graph shows that percentage of water accumulation increases gradually from January, May and September for every year except for 2019, with the least amount of water in the month of September. It clearly shows that flood geo-hazard is gradually increasing from September, 2017 (10.49345%) to May, 2018 (12.6057%) and a slight drop in May, 2019 (11.47714%). It shows that such geo-hazard event is gradually

increasing progressively over time with that of October, 2022 as high as (12.29319%). The number of scenes does not have any influence on the percentage of accumulated water but the total pixel as seen in Figure 4.1C with May 2018 having the maximum pixel of (3385141), then October, 2022 (3301221), May, 2019 (3082078) and September, 2017 (2817917).

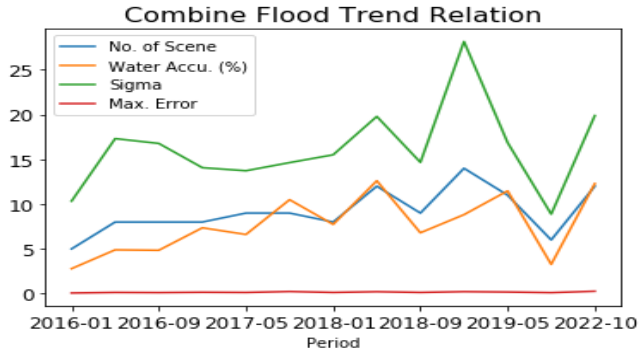

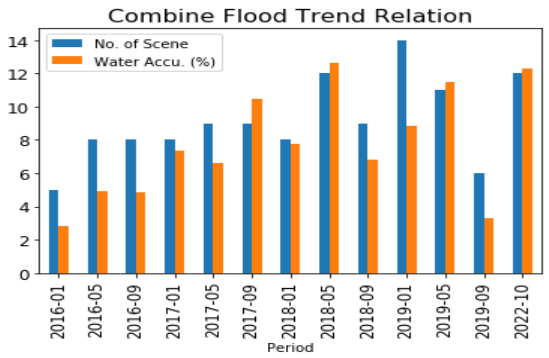

A

B

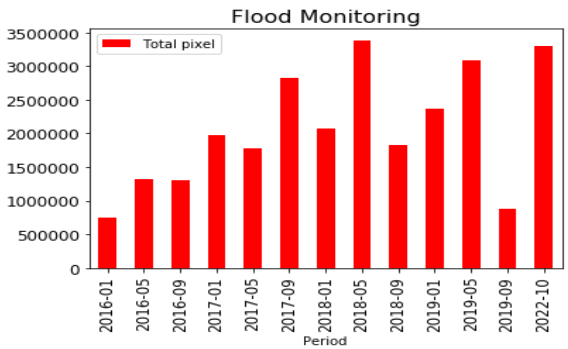

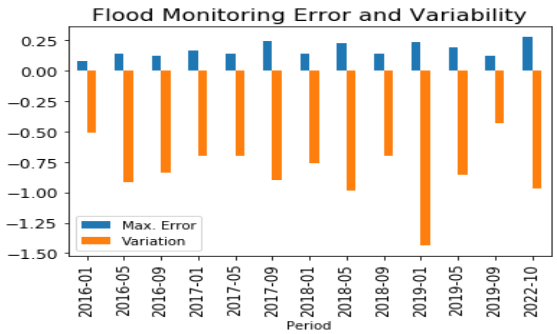

C

D

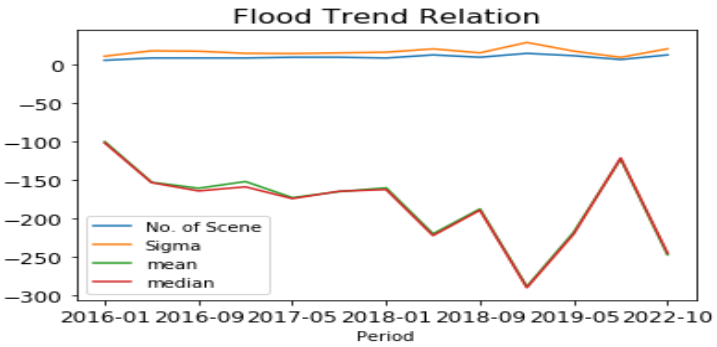

E

Figure 4.1 Result of Monthly flood event

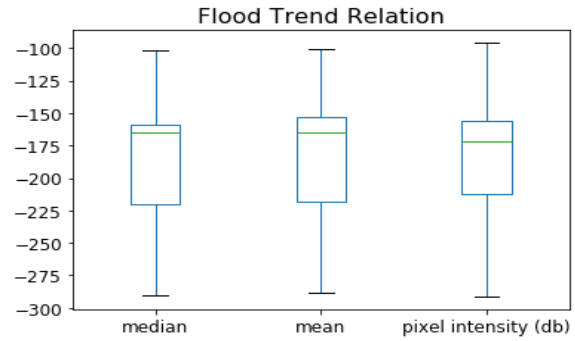

Period	*No. of Scene*	*Total pixel*	*mean*	*Sigma*	*Variation*	*Max. Error*	*Water Accu. (%)*	*Land Area (%)*
2016-01	5	750211	-100.502	10.3357	-0.5108	0.0737	2.79366	97.20634
2016-05	8	1314663	-153.224	17.3145	-0.9174	0.1403	4.895584	95.10442
2016-09	8	1301034	-161.013	16.778	-0.8373	0.121	4.844832	95.15517
2017-01	8	1975400	-152.282	14.0671	-0.7005	0.1595	7.356058	92.64394
2017-05	9	1774661	-173.246	13.7267	-0.7036	0.1372	6.608539	93.3914
2017-09	9	2817917	-165.362	14.6352	-0.8976	0.244	10.49345	89.5065
2018-01	8	2076873	-160.503	15.5076	-0.7607	0.1389	7.733926	92.26607
2018-05	12	3385141	-220.223	19.7895	-0.9871	0.2227	12.6057	87.3943
2018-09	9	1825972	-187.846	14.668	-0.7023	0.14	6.799613	93.20039
2019-01	14	2369905	-288.675	28.15251	-1.4351	0.22906	8.825128	91.17487
2019-05	11	3082078	-218.101	16.8713	-0.859	0.187	11.47714	88.5229
2019-09	6	878982	-122.814	8.8801	-0.4367	0.1168	3.273181	96.72682
2022-10	12	3301221	-247.33	19.8862	-0.9718	0.2741	12.29319	87.7068

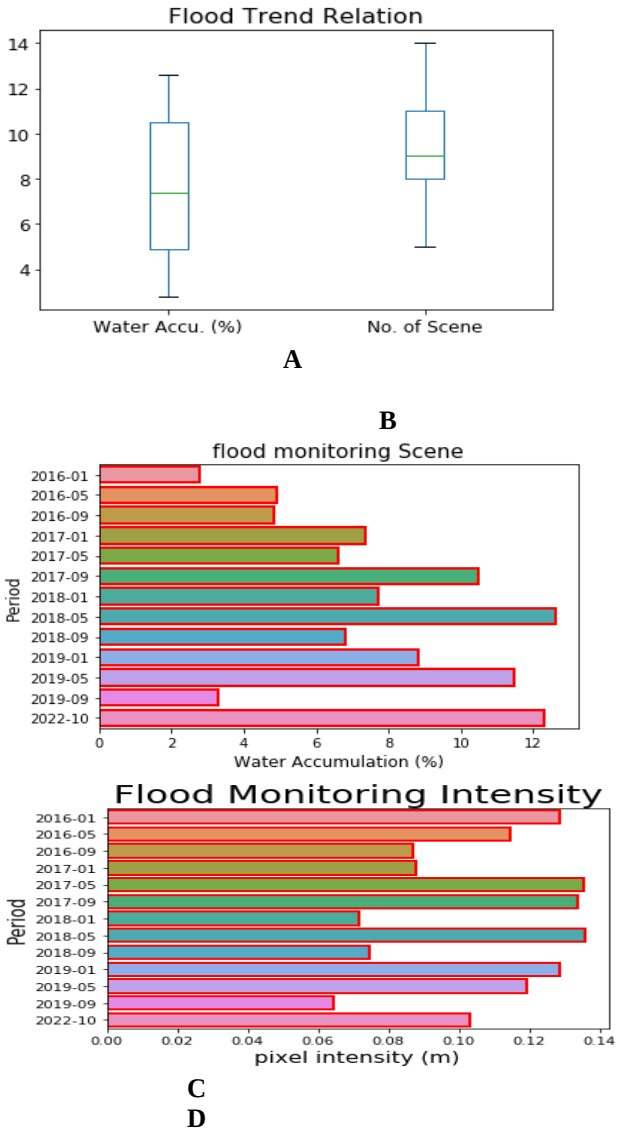

Figure 4.2 Monthly Correlation Flood Monitoring Event

The result of Figure 4.2 shows the trend relationship between the median, mean, pixel intensity (db), water accumulation and number of scenes using box plot. Figure 4.2A shows a high positive correlation between the median, mean and pixel intensity (db) as they all appear to be within the upper quartile of the box plot. Figure 4.2B shows a negative correlation between the number of scenes and the percentage accumulation of water with in the study area which indicated that, the number of scenes does not have any influence on the percentage of accumulated water. Figure 4.2C and D; show the flood vulnerability in terms of water shade in percentage over the study period at monthly interval.

Table 4.1 Percentage level of Water Accumulation area to Land Surface Area

It is evident that May, 2018 has the highest percentage of water shade area (12.6057%) with the highest percentage of flood geo-hazard events. Then October, 2020 (12.29319%), then May, 2019 (11.47714%) and September, 2017 (10.49345%) as shown in table 4.1.

Figure 4.3 Rate of Water Accumulation/Flood Event

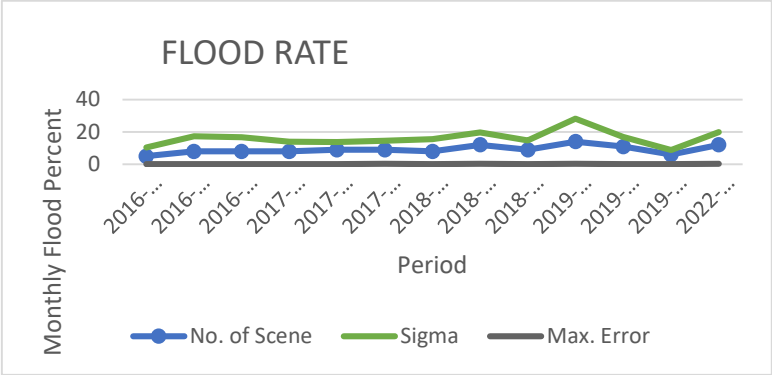

Figure 4.3; predict the rate of water accumulation over the study period of four (4) years with an extension to October, 2022, with the equation and an R^2 of less than one (1) as an indication of flood phenomenon. It shows a steady increase of flood geo-hazard over the study epoch at monthly intervals. It indicated a wide different with no stable increase associated with certain climatic and environmental factors which accelerate the rate of flood event. Below are maps of flood event over the study area at monthly interval.

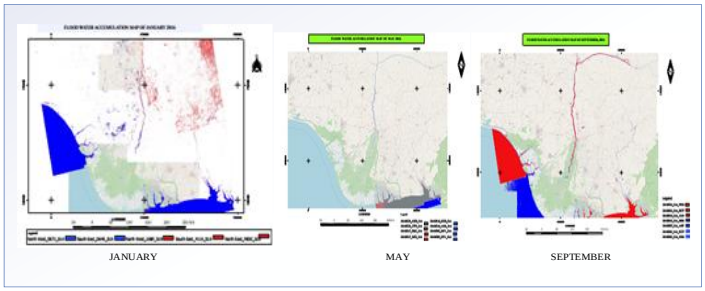

2016 Flood Event

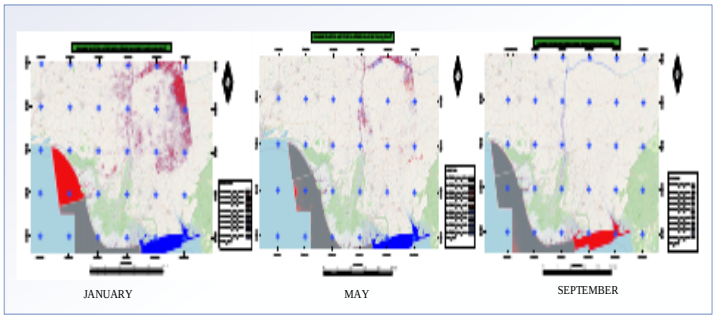

2017 Flood Event

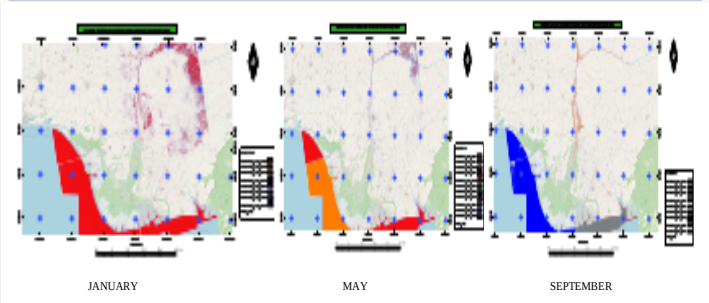

2018 Flood Event

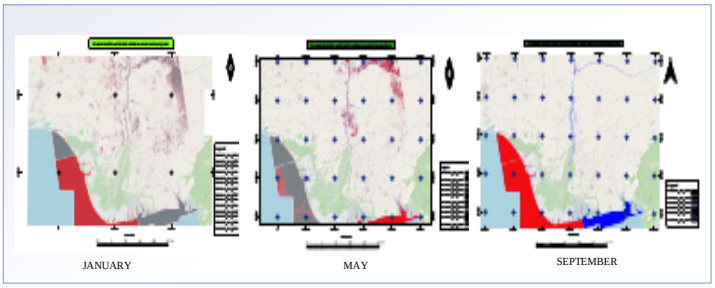

2019 Flood Event

4.2 Annual Flood Water Accumulation

The results of Figure 4.4 describe the annual flood water accumulation over the study area and period in relation to flood monitoring.

A

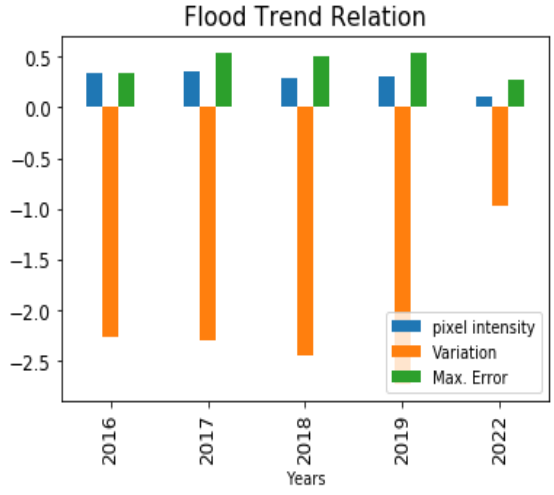

B

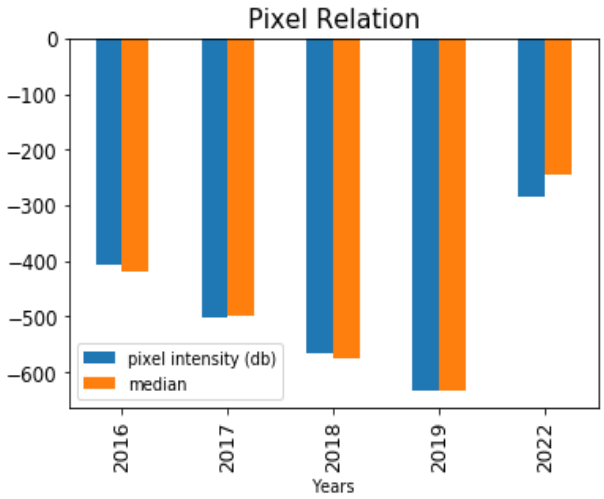

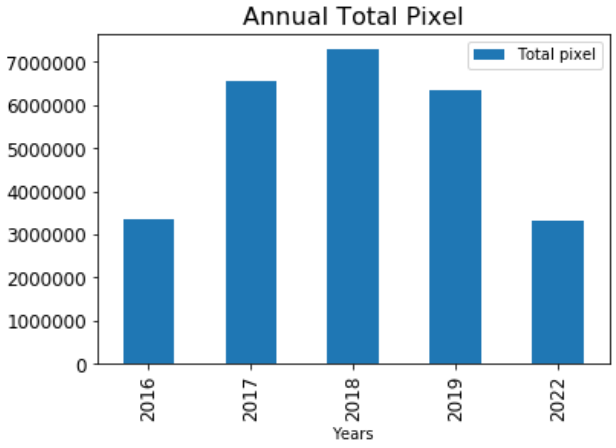

C

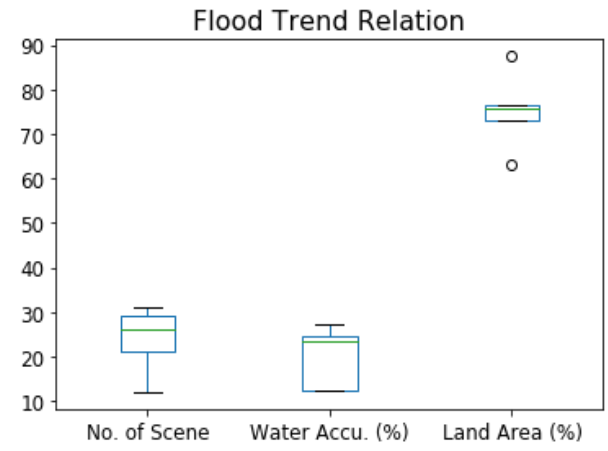

D

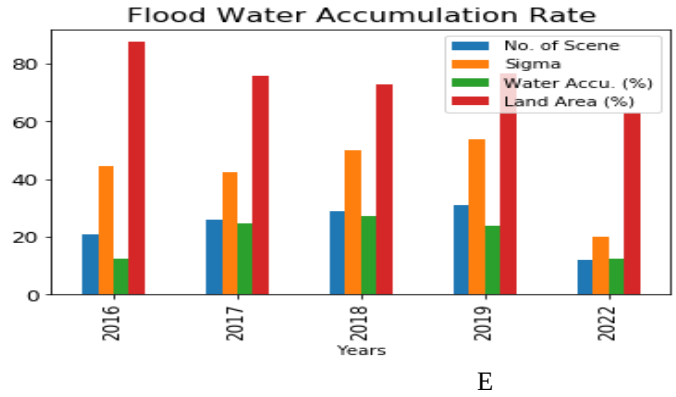

E

Figure 4.4 Result of Annual flood event

The Result of Figure 4.4A shows the outcome of the processing approach in terms of maximum error, coefficient of variation and active pixel intensity in relation to water accumulation with-in the study area over the study period. The range of maximum error incurred is less than 0.5 which shows that all signal outliers that would have affected the pixel intensity and variability have been eliminated to the barest minimum leaving only signals relating to the water body. With these, the flood water accumulation is highly quantified in decibel (db) showing regions with more accumulation within the study area over the study epoch. Figure 4.4B outlines the quantified intensity (db) with the estimated median value. This shows a strong correlation with both having the highest values in the same year. Year 2019 has the highest value, then 2018, with least value in 2022. The least value in 2022 is attributed to the fact that it was only one month's observation that was considered unlike that of other years which has a combination of three months of observation per year. Figure 4.4C shows the disparity in total pixel over the study period over the same study area. The study area is the same over the study period, but the total pixels differ because of the difference in flood water accumulation as it contributes to flood vulnerability. The range of annual total pixel in mixed descending order is 2018, 2017, 2019, 2016 and finally 2022. The first four years values were for three months, and that of the fifth year is for one month, which is why it has the least value, slightly below 2016, 2019, and 2017. Figure 4.4D was to investigate if there is a high correlation between water accumulation and number of processed scenes. From the box plot, it shows a very weak correlation, meaning that, the number of scenes is not a factor to the concentrated intensity of flood water accumulation over the study area and period. Meaning that, the numbers of scenes have no influence on the percentage water accumulation. Figure 4.4E shows the rate of flooded water accumulation of the study area and period. It is clear that, 2018, has the highest water accumulation rate, then 2017, 2019, 2016 and finally one month of 2022. Year 2022, is slightly below the previous years. Meaning that year 2022, would have been the highest if three months were considered or multiply the value of one month by a factor of 2.5 (2.5*12.29 = 30.725%), that is slightly above 2018 by three percent (3%).

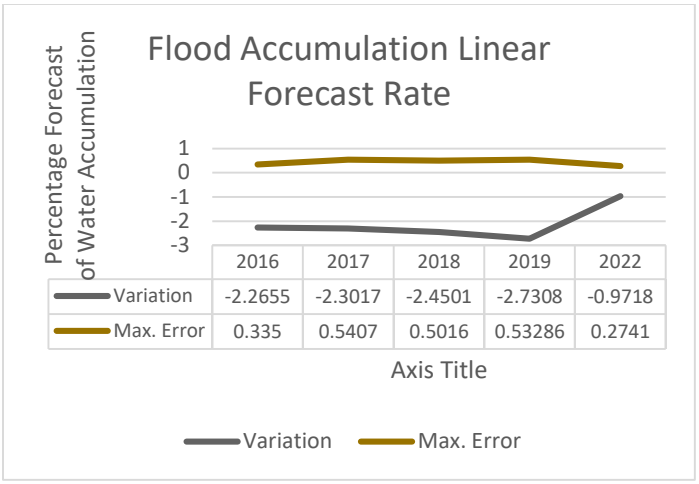

Figure 4.5 Rate of Flood Event to Land Area Linear Forecast

The annual flooded water accumulation rate in percentage is described in Figure 4.5. The two curves on the chart are for landed area with no flood event and that with flooded water accumulation with-in the study area over the study epoch. The curve in blue color represents areas with flood event having the least value of flood accumulation in 2016 and the highest in 2022 after being forecasted. The forecast was conducted using the curve slope rate. However, the slope rate is not uniform; therefore, the mean value was adopted as (2.76025%) increase over three years between 2019 and 2022. This value was adopted because the flood event displays a steady increase from 2016 to 2018 and slight depreciation in 2019. The prediction is based on the assumption that all contributing factors remains constant with regards to the mathematical variables used for the prediction. However, it is recommended that all contributing factors such as Slope, climate and weather parameters, anthropogenic be considered for proper flood prediction model and validation.

Table 4.2 Linear Flood Rate Forecast

Year	*Water Accu. (%)*	*Slope Rate (%)*
2016	12.53408	-
2016-2017	24.45805	11.924
2017-2018	27.13924	2.681
2018-2019	23.57545	-3.564
Mean value		2.76025

Table 4.3 Annual Percentage level of Water Accumulation to Land Surface Area

Years	*No. of Scene*	*pixel intensity*	*pixel intensity (db)*	*Total pixel*	*Mean*	*Sigma*	*median*	*Variation*	*Max. Error*	*Water Accu. (%)*	*Land Area (%)*
2016	*21*	*0.2993*	*-407.34*	*3365908*	*-414.7*	*44.4284*	*-420.3*	*-2.2655*	*0.335*	*12.53408*	*87.46592*

					4		2				
2017	26	0.3564 8	-500.23	656797 8	-49 0.89	42.429	-49 8.46	-2.30 17	0.5407	24.458 05	75.541 95
2018	29	0.2818 4	-566.63	728798 6	-56 8.57	49.9651	-57 4.47	-2.45 01	0.5016	27.139 24	72.860 76
2019	31	0.3123 6	-632.81	633096 5	-62 9.59	53.9039	-63 2.06	-2.73 08	0.5328 6	23.575 45	76.424 55
2022	12	0.1031 9	-284.08	330122 1	-24 7.33	19.8862	-24 5.36	-0.97 18	0.2741	30.725	69.275

Table 4.3 shows the percentage relationship of water accumulation to bare land with-in the study area over the study period in relation to other parameter obtained from the processing carried out with sentinel application toolbox (SNAP) version 8.0 updated.

Map of flood events from 2016 to 2019 were for three months interval (January, May and September) for days with data set at a twelve (12) repeat pass of sentinel -1 over the study area and period and part of 2022 for the month of October. They clearly show the concentration of water shade region within the study area, with year 2022 having the least concentration, followed by year 2016, then year 2019, then year 2017 and finally year 2018 having the highest concentration. The higher the concentration, the more prominent and severe to flood geo-hazard over the entire study area. The maps also show rapid rate of increase in flood event if nothing is done as a control measure, especially between year 2017 and year 2018. It proves that; once there is an occurrence of flood event in an area with no measure put in place for such occurrence, it will continue to repeat itself washing away vital part of the earth surface causing more havoc from year to year.

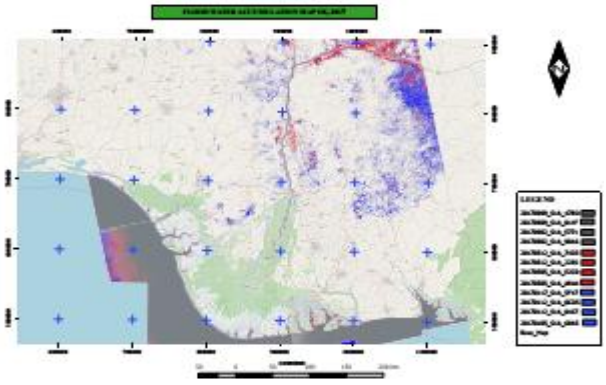

11 scene 2016 Flood Event
12 scene 2017 Flood Event

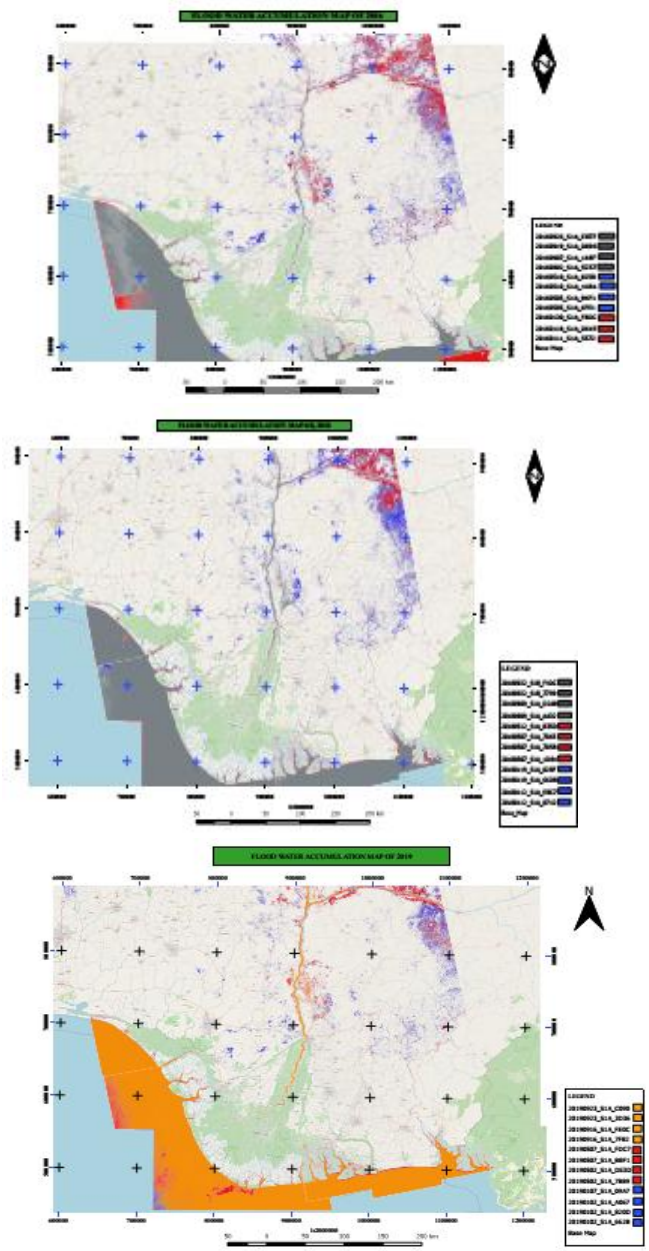

12 scene 2018 Flood Event
12 scene 2019 Flood Event
12 scenes of 2022 Flood Event

Figure 4.6 Annual Flood Water Accumulation Monitoring

5.0 Conclusion and Recommendation

This study has demonstrated that the Niger Delta Basin is experiencing a progressive and spatially expanding flood regime, driven by combination of hydro-climatic, geomorphological, and anthropogenic factors. Multi-temporal Sentinel-1 SAR analyses reveal a clear and concerning pattern: flooding is not an incidental or short-term phenomenon but a persistent and gradually intensifying environmental hazard. The peak inundation recorded in 2018, alongside significant flood coverage in 2017, 2019, and 2022, indicates that the region is

transitioning from seasonal, short-lived flood pulses to longer-duration and higher-magnitude inundation cycles. This behaviour strongly suggests a shift toward increased hydrological stress, possibly linked to extreme rainfall variability, land subsidence, river overflow, wetland degradation, and rising sea levels. The consistency of water detection across multiple SAR scenes and stable pixel intensity distributions confirms the reliability of radar-based monitoring in such humid and cloud-prone landscape. Moreover, the finding that the number of images does not significantly alter flood intensity estimates implies that flood progression is environmentally controlled, making Sentinel-1 an effective tool for ongoing surveillance.

Importantly, the documented flood expansion has direct implications on human settlements, agriculture, infrastructure, and socio-economic stability. Communities living along river channels and low-lying floodplains face increasing exposure to loss of property, displacement, health risks, and disruption of livelihoods. Agricultural zones, particularly farmlands that support food security are highly susceptible to prolonged inundation, leading to reduced yields and escalating food prices. Transportation routes, oil-and-gas facilities, markets, schools, and health centres are equally at risk. Without evidence-based intervention, the region may continue to experience heightened levels of vulnerability, environmental degradation, and economic loss.

Therefore, this study confirms that flooding in Niger Delta is not merely an environmental event but a growing human-security challenge, requiring proactive and coordinated action. The use of satellite-based flood monitoring is vital for guiding emergency response, supporting climate adaptation policies, and promoting resilience among local populations.

5.1 The following Recommendations are;

1. Government agencies (NEMA, NiMet, NASRDA), state emergency units, and local councils should jointly adopt a real-time radar-based flood monitoring framework to;

i. provide early warnings to risk communities

ii. support evacuation planning

iii. guide relief distribution

iv. reduce casualties and property loss.

2. Integrate flood maps into land-use planning and development control to restrict settlement expansion into high-risk zones and to ensure climate-resilient construction standards. New roads, schools, and housing estates should undergo flood vulnerability screening.

3. Strengthen community awareness and preparedness through local radio stations, community leaders, and disaster-management committees using the findings of the research to educate and sensitise residents.

4. Adopt Ecosystem-Based Flood Management. Wetlands, mangroves, and natural floodplains should be protected and restored, as they:

i. store excess water

ii. reduce flood peaks

iii. slow down flood progression

The research temporal maps clearly show where natural buffers have been degraded. Restoration efforts can help reduce severity.

5. Support Agricultural Planning and Food-Security Strategies. Farmers can use seasonal and long-term flood risk maps to:

i. adjust cropping calendars

ii. select flood-tolerant crop varieties

iii. optimise farm locations

Agricultural extension services should integrate satellite-based flood information into advisory programs.

6. Incorporate Flood Data into Energy and Oil Infrastructure Management. The Niger Delta hosts major oil and gas infrastructure. Refineries, pipelines, flow stations, and tank farms should:

i. conduct regular flood exposure assessments

ii. design elevated platforms where necessary

iii. develop flood-contingency plans based on SAR-derived flood histories

7. Promote Research, Data Sharing, and Capacity Building

Universities, research institutes, and governmental bodies should collaborate on:

i. hydrological modelling

ii. flood forecasting

iii. land subsidence monitoring

iv. climate vulnerability studies

Making flood datasets accessible improves planning efficiency and enhances community resilience.

Final, insights generated in this study provide a scientifically reliable basis for understanding and managing flood hazards in the Niger Delta. By integrating satellite technology with local planning and community action, stakeholders can significantly reduce vulnerability, enhance resilience, and support sustainable development for the millions of people who depend on this region for livelihood and security.

ACKNOWLEDGEMENT

The research diligently acknowledges effort of the developers of Sentinel data set obtained from Alaska satellite facilities and Sentinel Application Toolbox (SNAP) software provided by European Space Agency (ESA). The study wishes to acknowledge the center for Geodesy and Geodynamics for the used of their facilities.

Reference

Artiola, J., Pepper, I. L. and, & Brusseau, M. L. (2004). *Environmental Monitoring and Characterization*. University ofArizona, Tucson, AZ: Elsevier Science & Technology Books.

Benjamin, P. H., Kopp, R. E., Garner, A. J., Hay, C. C., Khan, N. S., Roy, K., & Shaw, T. A. (2018). Mapping Sea-Level Change in Time , Space , and Probability. *Annual Review Of Environment and Resources*, *43*(through 2050), 481–524.

Bioresita, F., & Puissant, A. (2021). Rapid Mapping of Temporary Surface Water using Sentinel-1 Imagery , case study : Zorn River flooding , Grand-Est , France. *Earth and Environmental Science*, (October), 2–6. https://doi.org/10.1088/1755-1315/731/1/012031

Bovenga, F. (2020). Special Issue "Synthetic Aperture Radar (SAR) Techniques and Applications." *Mdpi Sensors*, *1851*(March), 2–4. https://doi.org/10.3390/s20071851

Cazenave, A., & Gonéri, L. C. (2013). *Earth ' s Future Sea level rise and its coastal impacts Earth ' s Future*. 15–34. https://doi.org/10.1002/2013EF000188.Received

Clement, M. A. (2020). *Flood Extent and Volume Estimation using Multi-Temporal Synthetic Aperture Radar* . Newcastle University.

Earthdata Search , (2019). Greenbelt, MD: Earth Science Data and Information System (ESDIS) Projects, Earth Science Projects Division (ESPD), Flight Project Directorate, Goddard Space Flight Center (GSFC) National Aeronautics and Space Administration (NASA). URL: https://search.earthdata.nasa.gov/

Landuyt, L., Coillie, F. M. B. Van, Vogels, B., Dewelde, J., & Verhoest, N. E. C. (2021). Towards Operational Flood Monitoring in Flanders Using Sentinel-1. *IEEE Journal of Selected Topics in Applied Earth Observations and Remote Sensing*, *14*(November), 2–10. https://doi.org/10.1109/JSTARS.2021.3121992

Lee J. S. and Pottier E. (2009). Polarimetric SAR Radar Imaging: From Basic to Applications, CSR Press, Tylor & Francis Group.

Li, C., Dash, J., Asamoah, M., Sheffield, J., Dzodzomenyo, M., Gebrechorkos, S. H., … Wright, J. (2022). Increased flooded area and exposure in the White Volta river basin in Western Africa , identified from multi - source remote sensing data. *Scientific Reports*, (March), 1–8. https://doi.org/10.1038/s41598-022-07720-4

Martinis, S., Clandillon, S., Plank, S., Twele, A., Huber, C., Caspard, M., … Fuchs, E.-M. (2017). Advancing SAR and Optical Methods fpr Rapid Mapping. In *ASAPTERRA Final Report*. https://doi.org/No: 4000112375/14/I-NB

Matgen, P., Martinis, S., Wagner, W., Freeman, V., Zeil, P., & McCormick, N. (2020). *Feasibility assessment of an automated, global, satellite-based flood monitoring product for the Copernicus Emergency Management Service* (EUR 30073). https://doi.org/10.2760/653891

Rajakumari, S., Muthaiah, M. A. B., Meenambikai, M., Sarunjith, K. J., & Ramesh, R. (2021). Mapping of water logged areas using SAR images to assess the impact of Tropical Cyclone Gaja in Nagapattinam district , Tamil Nadu using Remote Sensing and GIS. *International Research Journal of Engineering and Technology (IRJET)*, *08*(02 | Feb 2021), 2–12. https://doi.org/p-ISSN: 2395-0072

Richards, M. A., Scheer, J. A., & William A. Holm. (2011). *Principles of Modern Radar* (Vol. I; D. R. and K. J. Kay, Ed.). Retrieved from http://www.scitechpub.com/

Sadek M., Li X., Mostafa E., Freeshah M., Kamal, A., Adou M. A. S., … Mustafa, E. K. (2020). Low-Cost Solutions for Assessment of Flash Flood Impacts Using Sentinel-1 / 2 Data Fusion and Hydrologic / Hydraulic Modeling : Wadi El-Natrun Region , Egypt. *Hindawi*, *2020*(February), 1–10. https://doi.org/10.1155/2020/1039309

World, B. G. (2016). *The Effect of Climate Change on Coastal Erosion in Wset Africa*. https://doi.org/WACA: West African Coastal Areas Management Program

Younis, M. (2015). Synthetic Aperture Radar (SAR): Principles and Applications. In *6th ESA Advance Training Course on Land Remote Sensing* (No. 82230). https://doi.org/82230 Oberpfaffenhofen, Germany

Article inflow

Received: 5th October, 2025

Accepted: 30th November, 2025

Published 31st December, 2025